# Profile of resonant photoelectron spectra versus the spectral function width and photon frequency detuning

R. Feifel,[1,2] V. Kimberg,[3] A. Baev,[3,4] F. Gel'mukhanov,[3,5] H. Ågren,[3] C. Miron,[1,6,7,*] G. Öhrwall,[1] M. N. Piancastelli,[1,8] S. L. Sorensen,[9] L. Karlsson,[1] and S. Svensson[1]

[1]*Department of Physics, Uppsala University, Box 530, S-751 21 Uppsala, Sweden*

[2]*Physical and Theoretical Chemistry Laboratory, Oxford University, South Parks Road, Oxford OX1 3QZ, United Kingdom*

[3]*Theoretical Chemistry, Roslagstullsbacken 15, Royal Institute of Technology, S-106 91 Stockholm, Sweden*

[4]*Institute for Lasers, Photonics and Biophotonics, The State University of New York at Buffalo, Buffalo New York 14260-3000, USA*

[5]*Institute of Automation and Electrometry, 630090 Novosibirsk, Russia*

[6]*Synchrotron SOLEIL, L'Orme des Merisiers, Saint-Aubin, Boîte Postale 48, 91192 Gif-sur-Yvette Cedex, France*

[7]*Laboratoire Francis Perrin, CNRS-URA 2453-DSM/DRECAM/SPAM CEA Saclay, Bâtiment 522, F-91191 Gif sur Yvette Cedex, France*

[8]*Department of Chemical Sciences and Technologies, University "Tor Vergata," I-00133 Rome, Italy*

[9]*Department of Synchrotron Radiation Research, Institute of Physics, University of Lund, Box 118, S-221 00 Lund, Sweden*

(Received 15 April 2004; published 22 September 2004)

The outermost, singly ionized valence state of $N_2$, the $X\ ^2\Sigma_g^+$ state, is investigated in detail as a function of the photon frequency bandwidth for core excitation to the N $1s \rightarrow \pi^*$ resonance, where the photon frequency is tuned in between the first two vibrational levels of this bound intermediate electronic state. We find a strong, nontrivial dependence of the resulting resonant photoemission spectral profile on the monochromator function width and the frequency of its peak position. For narrow bandwidth excitation we observe a well resolved vibrational fine structure in the final electron spectrum, which for somewhat broader bandwidths gets smeared out into a continuous structure. For even broader monochromator bandwidths, it converts again into a well resolved vibrational progression. In addition, spectral features appearing below the adiabatic transition energy of the ground state of $N_2^+$ are observed for broadband excitation. A model taking into account the interplay of the partial scattering cross section with the spectral function is presented and applied to the $X\ ^2\Sigma_g^+$ final state of $N_2^+$.

DOI: 10.1103/PhysRevA.70.032708 PACS number(s): 33.80.Eh, 33.70.Ca, 34.50.Gb

## I. INTRODUCTION

As has been shown in many experimental and theoretical studies before, the profiles of resonant photoelectron (RPE) spectra are strongly dependent on the photon frequency or on the detuning of the photon frequency relative to the photoabsorption resonance. One of the main reasons of such a strong dependence of the RPE profile on the detuning is a correspondence between the detuning and the scattering duration of the RPE process [1–4]. However, the spectral profile is very sensitive not only to the photon frequency, but also to the spectral function of the incident radiation. One of the most prominent related examples is the narrowing of the RPE resonances below the lifetime broadening when the bandwidth of the excitation light is small enough. This effect is commonly denoted in the literature as the resonant Auger Raman effect [5–7]. Another phenomenon directly related to the shape of the spectral function itself is a doubling of the RPE resonances under nonmonochromatic excitation which gives rise to additional spectral features under certain circumstances due to the imperfection of the spectral function [8–11].

Whereas, up to now, the role of the spectral function has been included in the description of the RPE spectra in the field of nonmonochromatic x-ray radiation on a hitherto adequate and successful level [1,8,10,12,13], a detailed analysis of the general role of the bandwidth on the RPE profile is lacking, in particular in the case of many-level systems like core-excited free molecules. The aim of the present article is to understand how the profile of RPE spectra is influenced by systematic changes of the bandwidth of the incident radiation at a fixed photon energy. As a showcase, the rather prominent resonant Auger decay of N $1s \rightarrow \pi^*$ core-excited $N_2$ molecules (see, e.g., Refs. [4,14–18]) is investigated for a photon energy tuned between the first two vibrational levels of the corresponding intermediate electronic state (see Refs. [19,20] and references therein). Excitation at this photon energy will be referred to as "valley excitation" in what follows. In particular, the evolution of the outermost singly ionized valence state of $N_2$, the $X\ ^2\Sigma_g^+$ state, is studied in detail for a systematically varied spectral function of the soft x-ray monochromator at that photon energy.

As is commonly known, the RPE spectral profile can be denoted as the product of the RPE spectrum for monochromatic excitation with the spectral function of the incident light. This intuitively often yields the impression that the only role of the spectral function is to broaden the spectral features of the resulting spectrum created by the monochromatic x-ray beam. In this article we will show that such a simple picture entirely breaks down in the case of valley excitation. In particular, for narrow bandwidth excitation we

*Also at MAX-LAB, University of Lund, Box 118, S-221 00 Lund, Sweden.

 

observe a well resolved vibrational fine structure in the final electron spectrum, which for somewhat broader bandwidths gets smeared out into a continuous structure, and which for even broader monochromator bandwidths converts again into a well resolved vibrational progression. The article is organized as follows. The experimental conditions and results of the measurements are presented in Secs. II and III, respectively. The general theory is outlined in Sec. IV. The physical picture of the role of the spectral function width on the RPE spectrum is elucidated in Sec. IV A. A detailed analysis of the role of the bandwidth of the incident radiation on the resonant photoelectron spectrum of the $N_2$ molecule is given in Sec. IV B. Our findings are summarized in the last section, Sec. V.

## II. EXPERIMENT

The experimental spectra were recorded at the undulator beamline I411 [21] at the MAX II storage ring at MAX-LAB, Lund, Sweden. This beamline is equipped with a modified Zeiss SX700 plane-grating monochromator covering the energy range 50 eV to 1200 eV, and with a rotatable SES 200 high-resolution electron spectrometer using a hemispherical analyzer. The main axis of the spectrometer lens was set to the "magic angle" (54.7°) with respect to the electric field vector of the linearly polarized synchrotron light, the spectrometer resolution was set to 75 meV full width at half maximum (FWHM) and the Doppler broadening is estimated to be 50 meV. In the present study, the monochromator spectral function was systematically varied by going from a very narrow ($2\gamma$=45 meV FWHM) to a very broad ($2\gamma$=1400 meV FWHM) bandwidth [corresponding to $\gamma$=22.5–700 meV half width at half maximum (HWHM); see Fig. 1 below], keeping the photon frequency fixed at 400.997 eV±10 meV (≈401 eV) in correspondence with the first valley between the $n=0$ and $n=1$ vibrational levels ("valley excitation") of the rich progression belonging to the N $1s\rightarrow\pi^*$ core-excited intermediate electronic state of $N_2$ (see, e.g., Ref. [20]; $n$ denotes here the vibrational quantum number in the core-excited state). $N_2$ gas with a stated purity of >99.99% was commercially obtained. The purity of the gas was carefully checked by on-line valence photoelectron spectroscopy during measurements. The absolute binding energy scale of the resonant Auger electron spectra is established on the grounds of the valence band spectrum presented in Ref. [22]. X-ray absorption spectra were recorded with high resolution around the N $1s\rightarrow\pi^*$ resonance in order to calibrate the photon energy absolutely before recording the individual electron spectra. The spectral function of the monochromator was experimentally characterized by separately recording the outer-valence Xe 5$p$ photoelectron lines at the fixed photon energy of 400.997 eV±10 meV (≈401 eV) as shown in Fig. 1. As we can see from this figure, the spectral function of the monochromator changes gradually from a Gaussian to an almost rectangular shaped function on going from small to large exit slit openings.

## III. RESULTS

In Fig. 2 we present a set of experimental data (left panel) of the singly ionized $X\ ^2\Sigma_g^+$ state of $N_2$, measured for a varying monochromator bandwidth at "valley excitation," along with the corresponding numerical simulations (right panel). The essential points of the simulations will be discussed below. As we can see from this figure, by going from a narrow monochromator bandwidth (22.5 meV HWHM) to somewhat larger bandwidths, the well resolved vibrational progression gets smeared out into an almost continuous band (≈105 meV HWHM), and for even broader bandwidths (≳115 meV HWHM) a well resolved vibrational progression appears again. In addition, the reappearing progression extends toward higher kinetic energies or lower binding energies (≳320 meV HWHM), giving rise to additional spectral features below the adiabatic $m=0$ vibrational line of the outermost $X\ ^2\Sigma_g^+$ singly ionized valence state of $N_2$, which are reminiscent of "hotbands" ($m$ denotes here the vibrational quantum number in the final electronic state). How can the disappearance and reappearance as well as the extension of the vibrational progression below the adiabatic transition of the outermost valence state be understood on the grounds of changes in the spectral function of the monochromator?

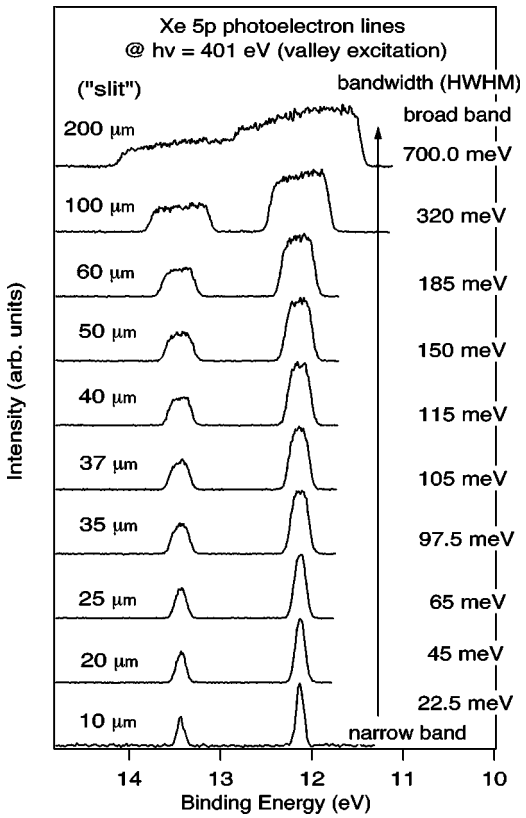


FIG. 1. The spectral function of the monochromator experimentally determined by measuring the outer valence Xe 5$p$ photoelectron lines at the photon energy of 401 eV (valley excitation).

## IV. GENERAL THEORY

In order to derive an adequate physical explanation of the experimental observations presented above, we will start from some basic equations. The RPE process is usually considered to be a one-step coherent scattering process which consists of core excitation and deexcitation leading to the

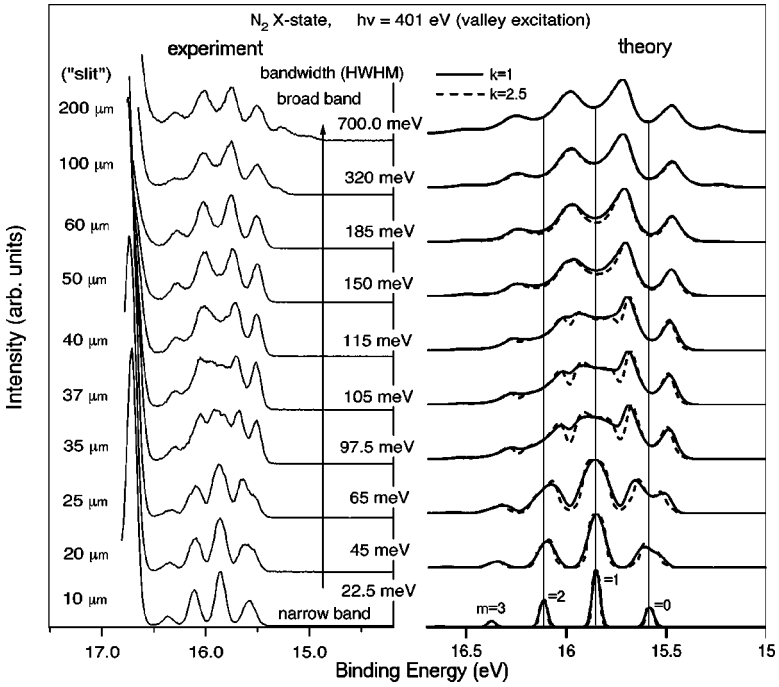


FIG. 2. The total RPE cross sections for the singly ionized $X$ state of the $N_2$ molecule upon valley excitation: $\omega=(\omega_{00}+\omega_{10})/2$. Comparison of the experimental and simulated spectra ($\Gamma=0.057$ eV).

emission of an Auger electron with kinetic energy $E$. To be consistent with the presentation of our measurements as shown in Fig. 2 we prefer to use the binding energy scale instead,

$$E_B = \omega - E, \tag{1}$$

where $\omega$ is the photon frequency. The total RPE cross section (in a.u.)

$$\sigma(E_B,\omega) = \sum_m \sigma_m(E_B,\omega) \tag{2}$$

is the sum of the partial RPE cross sections (corresponding to the final vibrational states $|m\rangle$), convoluted with the spectral function of the incident radiation $\Phi(\Omega,\gamma)$, which reads as [1]

$$\sigma_m(E_B,\omega) = |F_m|^2 \Phi(E_B - \omega_{fm,00},\gamma),$$

$$F_m = D\langle m|0\rangle + \sum_n \frac{\langle m|n\rangle\langle n|0\rangle}{\omega - E_B - \omega_{cn,fm} + \imath\Gamma}. \tag{3}$$

Here $\omega_{cn,fm}=\omega_{00}^{cf}+\varepsilon_n^c-\varepsilon_m^f$, $\omega_{fm,00}=\omega_{00}^{f0}+\varepsilon_m^f$, $\omega_{in,jm}=E_{i,n}-E_{j,m}$, where $E_{j,m}$ is the total energy of the electron-vibrational state $\Psi_{j,m}=\psi_j|m\rangle$; $\omega_{00}^{cf}$ and $\omega_{00}^{f0}$ are the resonant frequencies of an electron-vibrational transition between the lowest vibrational levels of the electronic states $c$ and $f$ and the electronic states $f$ and 0, respectively; $\Gamma$ is the lifetime width of the core-excited state. We neglect here the comparatively small lifetime width $\Gamma_f$ of the final state. Please note that the photon frequency $\omega$ in Eq. (3) is the frequency of the maximum of the spectral distribution of the x rays. The spectral function in Eq. (3) reaches its maximum value when $E_B=\omega_{fm,00}$, or $E=\omega-\omega_{fm,00}$. This reflects the energy conservation law of the whole RPE process [1].

The Kramers-Heisenberg scattering amplitude $F_m$ written in the Born-Oppenheimer approximation depends on the Franck-Condon (FC) amplitudes between the ground $|0\rangle$, core-excited $|n\rangle$, and final $|m\rangle$ vibrational states; it is known in the literature to describe accurately interference effects like, e.g., lifetime vibrational interference [14,23,24] and continuum-continuum interference [25–27]. We omit here a prefactor which depends on the electronic transition matrix elements. Furthermore, we will use atomic units and the notation $\varepsilon_n^c=\epsilon_n^c-\epsilon_0^c$, where $\epsilon_n^c$ is the vibrational energy of the core-excited state. For example, in the harmonic approximation $\varepsilon_n^i=n\omega_i$, where $\omega_i$ is the vibrational frequency of the $i$th electronic state. The relative amplitude $D$ of the direct photoemission process is neglected in the simulations. This is a reasonably good approximation for the singly ionized $X$ final state of $N_2$ for excitations on the $\pi^*$ resonance (cf. Ref. [4]). The spectral distribution of the incident x rays is conveniently described by the normalized spectral function

$$\Phi(\Omega,\gamma) = \frac{k}{\gamma_1\Gamma(1/2k)}\exp\left[-\left(\frac{\Omega}{\gamma_1}\right)^{2k}\right], \quad \gamma_1 = \frac{\gamma}{(\ln 2)^{1/2k}}, \tag{4}$$

with the half width at half maximum being equal to $\gamma$. Please note that $\Gamma(x)$ denotes here the analytical Gamma function and should not be confused with the notation of the core-hole lifetime used in Eq. (3) above. This expression of the spectral function is convenient for our simulations because it describes a smooth transition from a Gaussian ($k=1$) to a rectangular function ($k\gg1$) as can be seen from Fig. 3, where we explicitly plotted this function for three different values of the shape parameter $k$. The spectral function [cf. Eq. (4)] mimics the measured spectral distributions (cf. Fig. 1), save for the asymmetry of the experimental profile at $\gamma=320$ meV and $\gamma=700$ meV. We performed simulations of

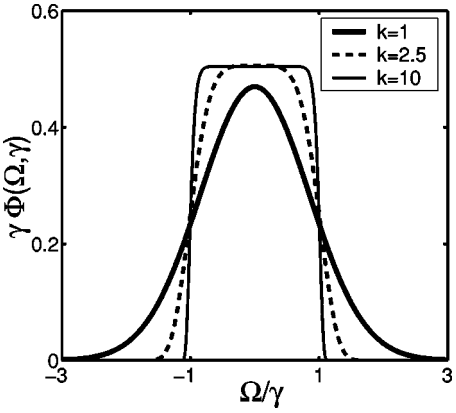


FIG. 3. The numerically implemented spectral function $\Phi(\Omega,\gamma)$ showing a smooth transition from a Gaussian ($k=1$) to a step function ($k\gg 1$) according to Eq. (4).

the RPE spectra for different values of the shape parameter $k$. The right panel of Fig. 2 displays the spectra for $k=1$ and $k=2.5$. The value $k=2.5$ comes closest to the experimentally observed rectangular shapes (see Fig. 3). One can see from Fig. 2, that both Gaussian ($k=1$) and rectangular ($k=2.5$) spectral functions give almost the same spectral profiles for $\gamma \geqslant 150$ meV. However, when the bandwidth $\gamma \leqslant 115$ meV, the simulations performed with a Gaussian spectral function fit the experiment better (cf. Fig. 2) than those based on a rectangular spectral function. This is in line with the measured spectral functions (cf. Fig. 1). The case of incident white light $[\Phi(\Omega,\gamma)=\Phi=\text{const}]$ deserves a special comment. Such broadband excitation gives basically the nonresonant Auger spectrum

$$\sigma_{\mathrm{NR}}(E_B,\omega) = \Phi \sum_m |F_m|^2, \tag{5}$$

because we coherently excite all intermediate state vibrational levels. It shows, contrary to resonant photoemission, linear dispersion on the binding energy scale, due to the linear dependence of the partial scattering amplitude $F_m$ on the frequency $\omega$ [cf. Eq. (3)]. It will be referred to as broadband excited Auger spectrum in what follows.

### A. Physical picture: A simplified four-level model

In order to gain a deeper insight into the physics it is helpful to start with the analysis of a simplified four-level system (see Fig. 4) for which the scattering amplitude reads as

$$F = F(\omega - E_B) = \frac{1}{\omega - E_B - \omega_{1f} + \imath\Gamma} + \frac{1}{\omega - E_B - \omega_{2f} + \imath\Gamma}. \tag{6}$$

Our model assumes core excitation from the ground state 0 to two core-excited states 1 and 2, with subsequent Auger decay to the single final state $f$. According to Eq. (6) the weights of these two scattering channels are the same. For the following discussion it is worthwhile to recapitulate the physical meaning of $|F|^2$: It is the spectral shape of broadband excited photoemission $\gamma=\infty$ [cf. Eq. (5)]. It is necessary to note that, according to Eq. (6), $F(E)=F(\omega-E_B)$ does not depend on the photon frequency $\omega$ on the (Auger) electron kinetic energy scale, but it depends on $\omega$ on the binding energy scale. Because we use the binding energy scale here, the "broadband excited spectrum" disperses when $\omega$ changes [cf. Eq. (6)], while the peak position of the spectral function $\Phi(E_B-\omega_{f0},\gamma)$ does not depend on the excitation energy. As a consequence, we can see that the major role of the spectral function is to select parts of the broadband excited spectrum $|F|^2$ around the resonant binding energy $E_B=\omega_{f0}$, according to $\sigma(E_B,\omega)=|F|^2\Phi(E_B-\omega_{f0},\gamma)$. This rather simple, but for the following discussion crucial, point is illustrated in Fig. 4. As we can see from this figure, there is a clear distinction between an "on-top" resonant excitation, $\omega=\omega_{10}$, and an excitation "between" two resonances (i.e., valley excitation), $\omega=(\omega_{10}+\omega_{20})/2$. When $\gamma$ is small both on-top and valley excitations lead to a single resonance in the resulting electron spectrum as indicated in this figure. The main difference is that the peak position of the spectral profile coincides with the line $1\rightarrow f$ of the broadband excited Auger spectrum in the case of on-top excitation ($\omega=\omega_{10}$). For valley excitation, the spectral function overlaps only with the valley between the lines $1\rightarrow f$ and $2\rightarrow f$ of the broadband excited Auger spectrum. Due to this, the on-top RPE spectrum shows only the narrow strong $1\rightarrow f$ peak while the valley spectrum consists of a weaker line situated between $1\rightarrow f$ and $2\rightarrow f$ of the broadband excited Auger spectrum. When $\gamma$ increases, a doubling of the resonance can be encountered for the valley excitation, with the same intensities of the blue and red shifted peaks. In addition, as indicated by Fig. 4(a)

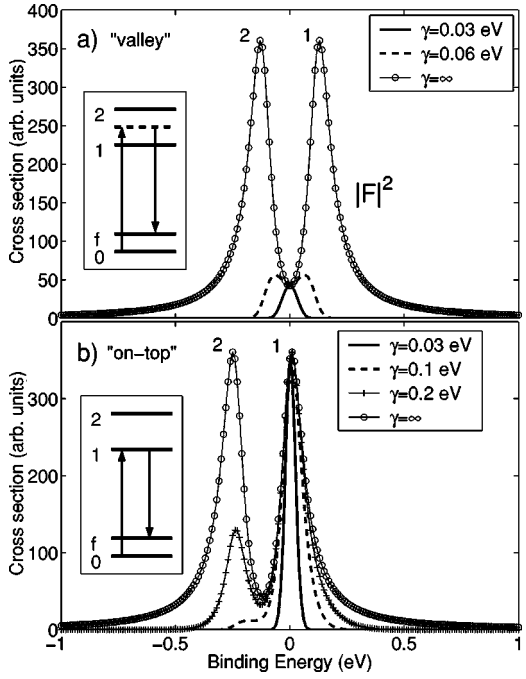


FIG. 4. Formation of the spectral profile for a four-level system for both resonant and valley excitations [$k=1$ (Gaussian)]. The binding energy ($E_B-\omega_{f0}$) is defined relative to $\omega_{f0}$. (a) Valley excitation, $\omega=(\omega_{10}+\omega_{20})/2$; (b) resonant excitation, $\omega=\omega_{10}$, $\Gamma=0.057$ eV, $\omega_{12}=0.24$ eV.

TABLE I. Spectroscopical constants used for calculations of the Morse potential curves and for the cross section simulations.

| | $\omega_e$ (cm$^{-1}$) | $\omega_e x_e$ (cm$^{-1}$) | $R^0$ (Å) | $E_{00}$ (eV) | Reference |
|---|---|---|---|---|---|
| $N_2$ ($X^1\Sigma_g^+$) | 2358.57 | 14.324 | 1.09768 | 0 | [28] |
| $N^*N$ ($^1\Pi_u$) | 1904.1 | 17.235 | 1.1645[a] | 400.88 | [20] |
| | 2207.00 | 16.10 | 1.11642 | 15.581 | [28] |

[a] $R_c$=1.1645 Å from Ref. [18].

the spacing between these two peaks increases with the increase of $\gamma$. This increase of the spacing is the key point to explain the above mentioned unusual evolution of the RPE spectrum of $N_2$ as a function of the bandwith. The picture looks different for on-top excitation: a small increase of $\gamma$ results in a weak red shoulder. This shoulder transforms to a peak for even larger $\gamma$ which moves toward the lower energy region and eventually becomes stronger [see Fig. 4(b)]. If $\gamma$ is large compared to the spacing between resonances 1 and 2, both on-top and valley excitations yield the same symmetrical double-peak profile. The reason for this is simple: now both excitations can basically be considered as off resonant due to the broad bandwidth of the excitation light, resulting in $|F|^2$.

From our discussion so far we can conclude the following. When the narrow spectral function is tuned to a certain part of the broadband Auger spectrum, the spectral function will cut out a narrow part of it. In turn, the spectral function selects a broader part from the broadband spectrum, when $\gamma$ increases. The RPE spectrum coincides with the broadband profile if $\gamma$ becomes comparable to or larger than the total width of the broadband Auger spectrum.

### B. Role of the spectral function width on the RPE profile of $N_2$: Detailed analysis of the total and partial cross sections

Numerical simulations were performed for the experimentally investigated $N_2$ case based on Eqs. (2) and (3) (see Fig. 2). The FC amplitudes were calculated using Morse potentials with the spectroscopic constants summarized in Table I. Figure 2 shows a direct comparison of the experimental and theoretical total RPE cross sections for the singly ionized $X$ final state of $N_2$. It is important to stress the major difference between the $N_2$ RPE spectra (cf. Fig. 2), which consist of many final vibrational states $|m\rangle$, and our simplified model system, which has only one final state (cf. Fig. 4). The reason for this difference lies in the partial cross sections $|F_m|^2\Phi(E_B-\omega_{fm,00},\gamma)$, which are different for different final vibrational states $|m\rangle$. More precisely, this difference is due to a strong dependence of $|F_m|^2$ (see Fig. 5) and the energy positions

$$E_B = \omega_{fm,00} \tag{7}$$

of the spectral function $\Phi(E_B-\omega_{fm,00},\gamma)$ on the final vibrational state $|m\rangle$. Our simulations show that only four final vibrational states ($m=0,1,2,3$) provide an essential contribution to the RPE spectral profile of $N_2$ (see Figs. 2 and 6).

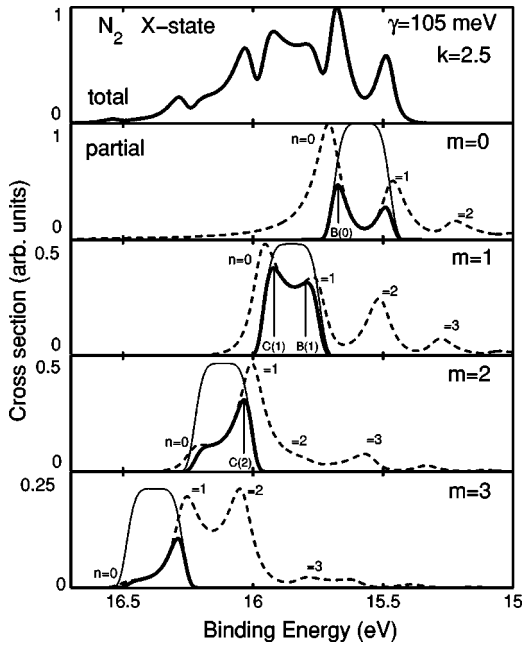


FIG. 5. Formation of the partial RPE cross sections for the singly ionized $X$ cationic state of the $N_2$ molecule upon valley excitation, $\omega=(\omega_{00}+\omega_{10})/2$; $\gamma=105$ meV. The upper panel shows the total RPE profile [cf. Eq. (2)]. The thin solid lines indicate the spectral function, the dashed lines represent the squared partial amplitude $|F_m|^2$, and the solid lines show the resulting partial RPE cross sections $\sigma_m(E_B,\omega)$ [cf. Eq. (3)]; $\Gamma=0.0575$ eV.

Consequently, the narrow spectral function ($\gamma=22.5$ meV) selects four peaks from the broadband excited Auger spectrum $\sigma_{NR}(E_B,\omega)$ [cf. Eq. (5)] which correspond to four final vibrational states ($m=0,1,2,3$) with different binding ener-

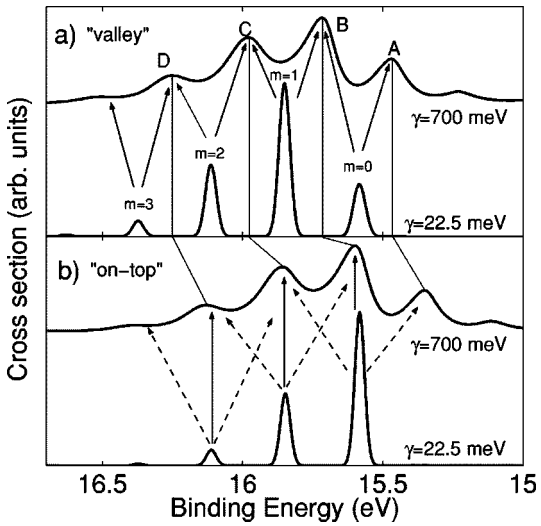


FIG. 6. Schematic depiction of the qualitative distinction between valley [$\omega=(\omega_{00}+\omega_{10})/2$,(a)] and on-top [$\omega=\omega_{00}$,(b)] RPE cross sections for the singly ionized $X$ state of the $N_2$ molecule. Simulations were performed with the Gaussian spectral function ($k=1$). The bandwidth $\gamma=700$ meV corresponds to the broadband excited Auger spectrum. The arrows show schematically the manifestation of the doubling effect for valley and on-top excitations.

gies $E_B=\omega_{f0,00}$, $\omega_{f1,00}$, $\omega_{f2,00}$, and $\omega_{f3,00}$. These peaks are marked by the label $m$ in Fig. 6(a). It is worth recapitulating that the spectral function selects only one peak in the simplified four-level model system above (cf. Fig. 4). Let us start our analysis from "auxiliary" Fig. 6, where we present spectra both for valley $[\omega=(\omega_{c0,00}+\omega_{c1,00})/2]$ and for on-top $(\omega=\omega_{c0,00})$ excitations. First of all, it is necessary to give an assignment for the main peaks *A*, *B*, *C*, and *D* of the broadband excited Auger spectrum (see spectra with $\gamma=700$ meV in Fig. 6). Peaks *A*, *B*, *C*, and *D* are formed mainly by the decay transitions $[1\rightarrow 0;2\rightarrow 1]$, $[0\rightarrow 0;1\rightarrow 1]$, $[0\rightarrow 1;1\rightarrow 2;2\rightarrow 3]$, and $[0\rightarrow 2;1\rightarrow 3]$, respectively. Here we used the notation $[n\rightarrow m]$ with $n$ and $m$ as the vibrational quantum numbers of the core-excited and final states, respectively. In other words, the *A*, *B*, *C*, and *D* features correspond to the decay transition with the following change of the vibrational quantum numbers $n-m=1,0-1,-2$, respectively. Thus, for on-top excitation [cf. Fig. 6(b)], the spectral functions $[\Phi(E_B-\omega_{fm,00},\gamma)]$ corresponding to the final states $m=0,1,2$ have maxima for the same binding energies as peaks *B*, *C*, and *D*, respectively, of the broadband excited Auger spectrum. For the valley excitation, the broadband excited Auger spectrum experiences a blue shift by half of a vibrational quantum as can be seen in Fig. 6(a). Here the peak positions of the spectral functions $[\Phi(E_B-\omega_{fm,00},\gamma)]$ coincide with the valleys of the broadband excited Auger spectrum. This difference between the on-top and valley excitations plays a crucial role in the formation of their RPE profile. The evolution of the RPE spectra from narrow ($\gamma=22.5$ meV) to broadband ($\gamma=700$ meV) excitation can therefore be explained as follows. Let us consider first the valley excitation [cf. Fig. 6(a)]: When $\gamma$ becomes larger, the spectral functions overlap more efficiently with the adjacent peaks of the broadband excited Auger spectrum. For example, the spectral functions $\Phi(E_B-\omega_{fm,00},\gamma)$ which correspond to the final states $m=0,1,2$ overlap with peaks *A* and *B*, *B* and *C*, *C* and *D*, respectively. Due to this overlap, the RPE peaks ($m=0,1,2$) corresponding to $\gamma=22.5$ meV start to split into two components. This can clearly be seen in both the experimental and the simulated spectra shown in Fig. 2.

The evolution of the spectrum for the on-top excitation [see Fig. 6(b)] is much simpler. In this case the manifestation of the doubling effect is considerably suppressed because the peak positions of the spectral functions coincide with the maxima of the broadband excited Auger spectra. Our simulations show that the only effect of the increase of $\gamma$ is the broadening and the redistribution of the intensities between the peaks *A*, *B*, *C*, and *D*, without change of their peak positions.

The evolution of the valley-excited experimental spectrum near 15.7 eV and 16.2 eV clearly shows a doubling of the spectral profile when the bandwidth is systematically changed from 22.5 meV to 700 meV (HWHM). Our simulations reproduce this trend very well (cf. Fig. 2) in accordance with the theory outlined here. However, the dynamics of the formation of the central part of the spectrum (i.e., the region around 15.8 eV) looks qualitatively different (cf. Fig. 2). As we can see from Fig. 2, the doubling effect is observed only for $\gamma>115$ meV in this region, but not for smaller bandwidths. To understand this finding on a more profound level, we shall analyze the partial cross sections $\sigma_m(E_B,\omega)$ [cf. Eq. (3)] for $\gamma=105$ meV which are displayed in Fig. 5. We see here the doubling effect for the partial cross sections, but not for the total cross section [cf. Eq. (2)]. The reason for this is the already mentioned dependence of the spacing between the components of the doublet on $\gamma$ (see Sec. IV A). For small bandwidths the peak positions of the adjacent components of the neighboring doublets are different (see Fig. 5):

$$E_B(B(0)) \neq E_B(B(1)), \quad E_B(C(1)) \neq E_B(C(2)). \tag{8}$$

Let us sum up the partial cross sections for $m=0,1,2$ as shown in Fig. 5. We get four peaks in the region $[15.6\ \text{eV}<E_B<16.1\ \text{eV}]$

$$B(0), \quad B(1), \quad C(1), \quad C(2). \tag{9}$$

This explains the rather complicated spectral shape of the central part of the spectrum (see Fig. 2 and upper panel of Fig. 5). As is apparent (see discussion in Sec. IV A, when $\gamma$ is large, the adjacent peaks coincide $[E_B(B(0))=E_B(B(1)),E_B(C(1))=E_B(C(2))]$ and we get two peaks instead of four; hence the doubling of the central part of the RPE spectra for $\gamma>115$ meV (cf. Fig. 2). Thus we have shown that under valley excitation each RPE peak exhibits doubling. The dependence on $\gamma$ of the spacing between the different components of such a doublet results in an unexpected and strong sensitivity to the bandwidth of the RPE spectral shape for a many-level system as can be found in molecules. Here we primarily studied the valley excitation (i.e., the photon energy was tuned between the first two vibrational levels $n=0,1$), and in addition compared it theoretically to an on-top excitation. In the case of valley excitation the role of the spectral function width is strongly emphasized. However, the influence of the width $\gamma$ of the spectral function on the formation of the spectral profile is also important for other photon energies. Furthermore, a similar behavior as discussed here for the singly ionized *X* final state of $N_2$ can be found for other final states, such as, e.g., the singly ionized *A* and *B* final states of $N_2$.

## V. SUMMARY

We found a strong dependence of the resonant photoemission spectral profile on the monochromator function width and the frequency of its peak position (carrier frequency). An intuitive picture tells us that the only role of the bandwidth is to broaden the profile of resonant photoemission. However, our investigations show that such a simplified consideration does not hold in general. Both experiment and theory demonstrate that the RPE profile of the $N_2$ molecule exhibits an unusual and strong dependence on the bandwidth of the spectral function for valley excitation. In particular, we observed a well resolved vibrational progression for small and large spectral function widths, which gets smeared out into a continuous structure for intermediate bandwidths. A model taking into account the interplay of the partial scattering cross sections with the spectral function was presented and successfully applied to the $X\ ^2\Sigma_g^+$ final state of $N_2^+$.

**ACKNOWLEDGMENTS**

The authors gratefully acknowledge the support from the Swedish National Research council (VR), the Swedish Foundation for Strategic Research (SSF), and the Swedish Foundation for International Cooperation in Research and Higher Education (STINT). Two of the authors (R.F. and A.B.) would in particular like to thank VR and STINT for financial support of their stay at the Theoretical and Physical Chemistry Laboratory at Oxford University, United Kingdom, and at the Institute for Lasers, Photonics and Biophotonics, the State University of New York at Buffalo, USA, respectively. The collaboration of the staff of MAX-LAB is gratefully acknowledged.

[1] F. Gel'mukhanov and H. Ågren, Phys. Rep., **312**, 87 (1999).
[2] M. N. Piancastelli, J. Electron Spectrosc. Relat. Phenom., **107**, 1 (2000).
[3] S. L. Sorensen and S. Svensson, J. Electron Spectrosc. Relat. Phenom., **114-116**, 1 (2001).
[4] R. Feifel, A. Baev, F. Gel'mukhanov, H. Ågren, M.-N. Piancastelli, M. Andersson, G. Öhrwall, C. Miron, M. Meyer, S. L. Sorensen, A. Naves de Brito, O. Björneholm, L. Karlsson, and S. Svensson, Phys. Rev. A, **69**, 022707 (2004).
[5] P. Eisenberger, P. M. Platzman, and H. Winnik, Phys. Rev. Lett., **36**, 623 (1976).
[6] G. S. Brown, M. H. Chen, B. Crasemann, and G. E. Ice, Phys. Rev. Lett., **45**, 1937 (1980).
[7] A. Kivimäki, A. Naves de Brito, S. Aksela, H. Aksela, O.-P. Sairanen, A. Ausmees, S. J. Osborne, L. B. Dantas, and S. Svensson, Phys. Rev. Lett., **71**, 4307 (1993).
[8] F. Gel'mukhanov and H. Ågren, Phys. Lett. A, **193**, 375 (1994).
[9] S. Aksela, E. Kukk, H. Aksela, and S. Svensson, Phys. Rev. Lett., **74**, 2917 (1995).
[10] G. B. Armen and H. Wang, Phys. Rev. A, **51**, 1241 (1995).
[11] R. Feifel, A. Baev, F. Gel'mukhanov, H. Ågren, M. Andersson, G. Öhrwall, M. N. Piancastelli, C. Miron, S. L. Sorensen, A. Naves de Brito, O. Björneholm, L. Karlsson, and S. Svensson, J. Electron Spectrosc. Relat. Phenom., **134**, 49 (2004).
[12] E. Pahl, H.-D. Meyer, and L. S. Cederbaum, Z. Phys. D: At., Mol. Clusters **38**, 215 (1996).
[13] Z. W. Gortel, R. Teshima, and D. Menzel, Phys. Rev. A **58**, 1225 (1998).
[14] M. Neeb, J.-E. Rubensson, W. Biermann, and W. Eberhardt, J. Electron Spectrosc. Relat. Phenom. **67**, 261 (1994).
[15] M. N. Piancastelli, A. Kivimäki, B. Kempgens, M. Neeb, K. Maier, U. Hergenhahn, A. Rüdel, and A. Bradshaw, J. Electron Spectrosc. Relat. Phenom., **98-99**, 111 (1999).
[16] M. N. Piancastelli, R. F. Fink, R. Feifel, M. Bässler, S. L. Sorensen, C. Miron, H. Wang, I. Hjelte, O. Björneholm, A. Ausmees, S. Svensson, P. Sałek, F. Kh. Gel'mukhanov, and H. Ågren, J. Phys. B, **33**, 1819 (2000).
[17] R. Feifel, F. Gel'mukhanov, A. Baev, H. Ågren, M. N. Piancastelli, M. Bässler, C. Miron, S. L. Sorensen, A. Naves de Brito, O. Björneholm, L. Karlsson, and S. Svensson, Phys. Rev. Lett., **89**, 103002 (2002).
[18] A. Baev, R. Feifel, F. Gel'mukhanov, H. Ågren, M. N. Piancastelli, M. Bässler, C. Miron, S. L. Sorensen, A. Naves de Brito, O. Björneholm, L. Karlsson, and S. Svensson, Phys. Rev. A, **67**, 022713 (2003).
[19] K. C. Prince, M. Vondracek, J. Karvonen, M. Coreno, R. Camilloni, L. Avaldi, and M. de Simone, J. Electron Spectrosc. Relat. Phenom., **101-103**, 141 (1999).
[20] R. Feifel, M. Andersson, G. Öhrwall, S. L. Sorensen, M.-N. Piancastelli, M. Tchaplyguine, O. Björneholm, L. Karlsson, and S. Svensson, Chem. Phys. Lett., **383**, 222 (2004).
[21] M. Bässler, A. Ausmees, M. Jurvansuu, R. Feifel, J.-O. Forsell, P. de Tarso Fonseca, A. Kivimäki, S. Sundin, S. L. Sorensen, R. Nyholm, O. Björneholm, S. Aksela, and S. Svensson, Nucl. Instrum. Methods Phys. Res. A, **469**, 382 (2001).
[22] P. Baltzer, L. Karlsson, and B. Wannberg, Phys. Rev. A, **46**, 315 (1992).
[23] F. Gel'mukhanov, L. Mazalov, and A. Kondratenko, Chem. Phys. Lett., **46**, 133 (1977).
[24] T. X. Carroll, M. Coville, P. Morin, and T. D. Thomas, J. Chem. Phys., **101**, 998 (1994).
[25] P. Sałek, F. Kh. Gel'mukhanov, and H. Ågren, Phys. Rev. A, **59**, 1147 (1999).
[26] Z. W. Gortel, R. Teshima, and D. Menzel, Phys. Rev. A, **60**, 2159 (1999).
[27] R. Feifel, F. Burmeister, P. Salek, M.-N. Piancastelli, M. Bässler, S. L. Sorensen, C. Miron, H. Wang, I. Hjelte, O. Björneholm, A. Naves de Brito, F. Kh. Gel'mukhanov, H. Ågren, and S. Svensson, Phys. Rev. Lett., **85**, 3133 (2000).
[28] K. P. Huber and G. Herzberg, *Molecular Spectra and Molecular Structure IV, Constants of Diatomic Molecules* (Van Nostrand Reinhold, New York, 1979).